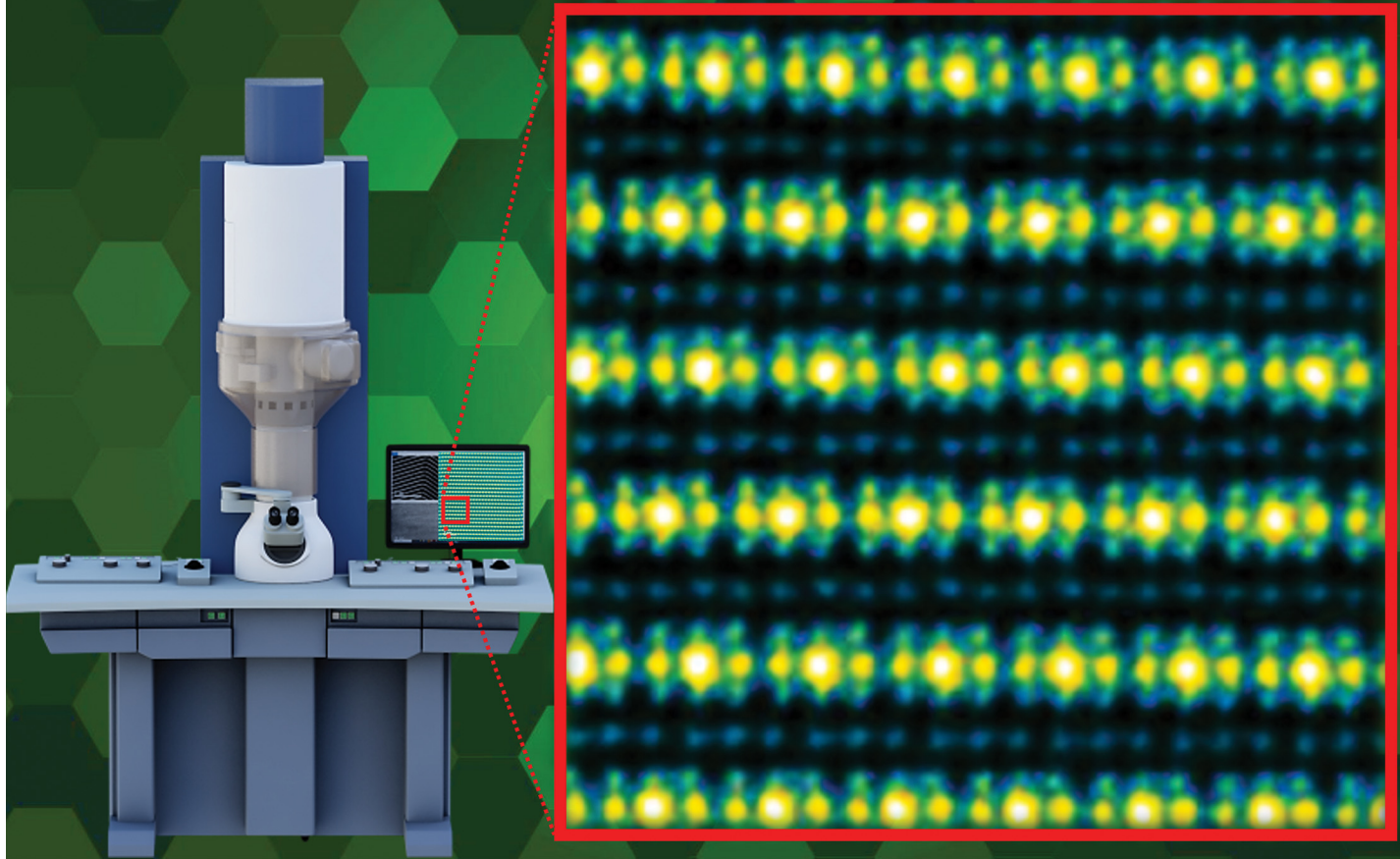


# Optimum Bright-Field



Showcasing research from the National Institute of Advanced Industrial Science and Technology (AIST) and Sumika Chemical Analysis Service (SCAS), Ltd., Japan.

Probing the atomic arrangement of honeycomb layered oxides *via* optimum bright-field scanning transmission electron microscopy (OBF-STEM)

This study employs highly dose-efficient, atomic-resolution optimum bright-field scanning transmission electron microscopy (OBF-STEM), enabling the probing of atomic arrangements in honeycomb-layered oxides. The successful application of OBF-STEM facilitates the structural characterisation of electron-beam-sensitive honeycomb-layered oxide materials, thereby advancing the frontier of observation techniques for the effective investigation of emergent physicochemical phenomena.

Image reproduced by permission of Titus Masese, Godwill Mbiti Kanyolo, Yoshinobu Miyazaki, Kimiya Sukegawa and Tomohiro Saito from *Phys. Chem. Chem. Phys.*, 2025, **27**, 14729.

## As featured in:



See Titus Masese,  
Godwill Mbiti Kanyolo *et al.*,  
*Phys. Chem. Chem. Phys.*,  
2025, **27**, 14729.



Cite this: *Phys. Chem. Chem. Phys.*,  
2025, 27, 14729

Received 27th March 2025,  
Accepted 8th June 2025

DOI: 10.1039/d5cp01190f

rsc.li/pccp

## Probing the atomic arrangement of honeycomb layered oxides via optimum bright-field scanning transmission electron microscopy (OBF-STEM)†

Titus Masese, \*<sup>a</sup> Godwill Mbiti Kanyolo, \*<sup>a</sup> Yoshinobu Miyazaki,<sup>b</sup> Kimiya Sukegawa<sup>b</sup> and Tomohiro Saito<sup>b</sup>

Here, we employ low-dose atomic resolution optimum bright-field (OBF) scanning TEM (STEM) to maximise the signal-to-noise ratio, enabling the probing of the arrangement of atoms in honeycomb-layered  $\text{Na}_2\text{Zn}_2\text{TeO}_6$  (precursor). This successful application of OBF-STEM facilitates the characterisation of local atomic structures in electron-beam-sensitive honeycomb-layered materials, thereby pushing the frontier of such observation techniques towards investigating a postulate linking the hexagonal lattice of such precursors to precluded silver bilayered structures upon topotactic ion exchange reaction with molten Ag salt.

Honeycomb-layered oxides, comprising alkali or coinage metal atoms interspersed between layers of transition or heavy metal atoms arranged in a honeycomb pattern, have garnered significant interest across diverse fields, including electrochemistry, materials science, and condensed matter physics.<sup>1</sup> The distinctive honeycomb arrangement of both transition metal and alkali metal atoms endows these materials—particularly honeycomb-layered tellurates—with remarkable physicochemical properties such as fast ionic conduction, high voltage electrochemical performance, exotic topologies, and magnetic behaviour coupled with other diverse crystal chemistries.<sup>1–3</sup>

The honeycomb arrangement of mobile alkali metal atoms, exemplified in honeycomb-layered tellurates such as  $\text{Na}_2\text{M}_2\text{TeO}_6$  ( $\text{M} = \text{Ni}, \text{Co}, \text{Mg}, \text{Zn}, \text{Cu}$ , etc.) and  $\text{K}_2\text{M}_2\text{TeO}_6$  ( $\text{M} = \text{Ni}, \text{Co}, \text{Mg}$ ),<sup>3–5</sup> gives rise to emergent phenomena when these alkali metal atoms undergo topotactic exchange with coinage metal atoms like Ag.<sup>3,6,7</sup> Specifically, Ag-based honeycomb layered materials are known to exhibit peculiar fractional Ag valency

states,  $\text{Ag}^{1/2+}$ ,  $\text{Ag}^{2/3+}$  etc. thought to arise from exotic phenomena (such as argentophilic bilayers) albeit inconspicuously absent in alkali-metal (Li, Na, K, etc.)-based honeycomb layered materials. In addition to the usual non-chiral/ $U(1)$  structure of valence electrons (and holes) on 2D lattices, theoretical considerations place the origin of these fractional valencies to an emergent chiral (pseudo-spin)/ $SU(2)$  structure *via* *sd*-hybridisation of silver orbitals on the honeycomb lattice—a theoretical formulation analogous to *sp*-hybridisation of carbon orbitals on the honeycomb lattice of graphene.<sup>7</sup>

As a result, a necessary postulate for the validity of the pseudo-spin/ $SU(2) \times U(1)$  model is the link between the honeycomb lattice and exhibited bilayered structures of silver.<sup>3,6,7</sup> In particular, experiments involving the honeycomb lattice and topotactic exchange of alkali metal atoms (e.g., Na) with  $\text{Ag}^{Q'=+1}$  ion in precursor compounds such as  $\text{Na}_2\text{M}_2\text{TeO}_6$  ( $\text{M} = \text{Ni}, \text{Co}, \text{Mg}, \text{Cu}, \text{Zn}$ ) or  $\text{K}_2\text{M}_2\text{TeO}_6$  ( $\text{M} = \text{Ni}, \text{Co}, \text{Mg}$ ) are expected to report domains predominantly featuring argentophilic  $\text{Ag}^{Q'=+1/2}$  bilayers (postulate trend 1: “honeycomb = bilayers”) with fractional charge (*i.e.*,  $Q = +1 \rightarrow Q' = +1/2$ ). Conversely, experiments involving topotactic  $\text{Ag}^{Q'=+1}$  ion exchange on non-honeycomb lattices such as the ubiquitous triangular (hexagonal) lattice are expected to report domains predominantly featuring non-argentophilic  $\text{Ag}^{Q'=+1}$  monolayers (*i.e.*,  $Q = +1 \rightarrow Q' = +1$ ), since the postulate requires non-honeycomb lattices to preclude the formation of argentophilic bilayers (postulate trend 2: “hexagonal = monolayers  $\neq$  bilayers”).

As such, postulate trend 1 was succinctly observed and reported for  $\text{Ag}_x\text{M}_2\text{TeO}_6$  by the present authors *et al.*<sup>6–8</sup> Consequently, it would be extremely insightful to also unambiguously observe postulate trend 2, lending further credence to the honeycomb postulate relied upon by the pseudo-spin/ $SU(2) \times U(1)$  model.<sup>3,6,7</sup> Conversely, finding and reporting a predominantly silver-bilayered structure after topotactic silver-ion exchange on a non-honeycomb lattice could serve as a counter-example falsifying and/or contradicting the honeycomb postulate, thus prompting a reconsideration of the

<sup>a</sup> Research Institute of Electrochemical Energy, National Institute of Advanced Industrial Science and Technology (AIST), 1-8-31 Midorigaoka, Ikeda, Osaka 563-8577, Japan. E-mail: titus.masese@aist.go.jp, titusmasese@gmail.com, gm.kanyolo@aist.go.jp, gmkanyolo@gmail.com, gmkanyolo@mail.uec.ac.jp

<sup>b</sup> Tsukuba Satellite Laboratory, Sumika Chemical Analysis Service (SCAS), Ltd., Tsukuba, Ibaraki 305-8565, Japan

† Electronic supplementary information (ESI) available. See DOI: <https://doi.org/10.1039/d5cp01190f>

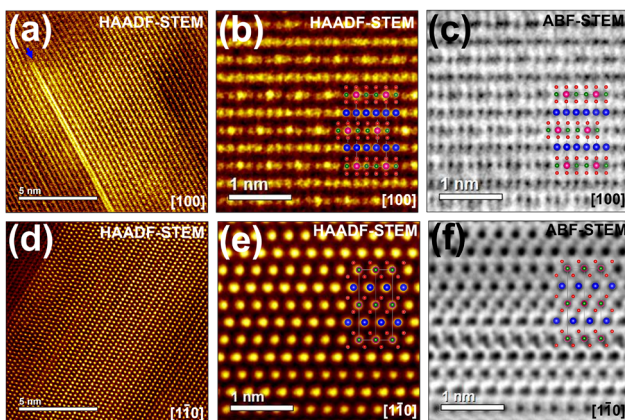


**Fig. 1** High-resolution scanning transmission electron microscopy (STEM) imaging along multiple zone axes of  $\text{Ag}_2\text{Zn}_2\text{TeO}_6$  (prepared via topochemical reaction of  $\text{Na}_2\text{Zn}_2\text{TeO}_6$  with  $\text{AgNO}_3$  at  $250^\circ\text{C}$  for 99 hours in air). (a) High-angle annular dark-field (HAADF)-STEM image of  $\text{Ag}_2\text{Zn}_2\text{TeO}_6$  taken along [100] zone axis. Whilst a Ag atom bilayer domain is shown in blue arrow, the Ag-lattice is predominantly monolayered. (b) and (c) Magnified HAADF- and (annular bright-field) ABF-STEM images of  $\text{Ag}_2\text{Zn}_2\text{TeO}_6$  taken along [100] zone axis. (d) HAADF-STEM image of  $\text{Ag}_2\text{Zn}_2\text{TeO}_6$  taken along [110] zone axis. (e) and (f) Magnified HAADF- and ABF-STEM images of  $\text{Ag}_2\text{Zn}_2\text{TeO}_6$  taken along [110] zone axis. Ag atoms are shown in blue whilst Ni and Te atoms are shown in green and pink, respectively. Oxygen atoms are shown in red.

theoretical foundations of not only the pseudo-spin/ $SU(2) \times U(1)$  model but also other closely related bond theoretic models relevant to silver-based honeycomb layered materials.<sup>3</sup>

Fig. 1 presents high-resolution scanning transmission electron microscopy (STEM) images of  $\text{Ag}_2\text{Zn}_2\text{TeO}_6$ , synthesised via topotactic ion exchange of Na atoms in  $\text{Na}_2\text{Zn}_2\text{TeO}_6$  with Ag. Details about the synthesis of  $\text{Ag}_2\text{Zn}_2\text{TeO}_6$  are provided in the ESI.† Crucially, most of the observed domains reveal Ag monolayer arrangements (Fig. 1a and b) in accordance with postulate trend 2, contrary to Ag bilayers that would align in a honeycomb lattice configuration if the replaced Na atoms in  $\text{Na}_2\text{Zn}_2\text{TeO}_6$  were initially arranged in a honeycomb pattern *i.e.* the converse of postulate trend 1. This observation suggests that a significant portion of the Na atoms in the precursor  $\text{Na}_2\text{Zn}_2\text{TeO}_6$  are not arranged in a honeycomb lattice. Whilst it is conventional to ascertain the type of lattice arrangement *via* standard scanning transmission electron microscopy (STEM), particularly high-angle annular dark-field (HAADF)-STEM and annular bright-field (ABF)-STEM, as is evident in the standard STEM images of  $\text{Na}_2\text{Zn}_2\text{TeO}_6$  (Fig. S1, ESI†), clarity is severely hindered by electron beam damage. Thus, unlike many honeycomb layered oxides with reported atomic-resolution observations,  $\text{Na}_2\text{Zn}_2\text{TeO}_6$  is particularly vulnerable to electron beam damage,<sup>9</sup> likely due to its solid electrolyte properties, including high ionic conductivity and low electrical conductivity.<sup>9,10</sup>

Thus, atomic-resolution imaging of beam-sensitive materials presents a persistent challenge for standard electron microscopy. By contrast, optimum bright-field (OBF) STEM—a non-standard low-electron-dose imaging technique—offers a breakthrough by achieving high signal-to-noise ratio images with markedly improved dose efficiency compared to

conventional methods.<sup>11,12</sup> This enables superior imaging with reduced irradiation damage and enhanced spatial resolution. However, observing the atomic structure using OBF-STEM requires thinning the sample to less than approximately 10 nm to satisfy the weak phase object approximation.<sup>13</sup> This poses significant challenges for focused ion beam (FIB) processing and likely accounts for the lack of reported OBF-STEM observations on solid-state electrolytes, including layered oxides.

In this study, OBF-STEM was effectively utilised to directly visualise the local arrangement of Na atoms in  $\text{Na}_2\text{Zn}_2\text{TeO}_6$ , revealing that the Na atoms are predominantly arranged in a hexagonal lattice. The ascertained hexagonal lattice accounts for the observed monolayer arrangement of Ag atoms in  $\text{Ag}_2\text{Zn}_2\text{TeO}_6$  synthesised *via* topotactic ion exchange using molten  $\text{AgNO}_3$  with  $\text{Na}_2\text{Zn}_2\text{TeO}_6$  (in stark contrast to the recently reported bilayer arrangement of Ag atoms in *e.g.*  $\text{Ag}_6\text{Ni}_2\text{TeO}_6$  after topotactic ion exchange with *e.g.*  $\text{K}_2\text{Ni}_2\text{TeO}_6$ , with K atoms arranged instead in a honeycomb lattice<sup>3,6</sup>), thus lending credence to the honeycomb postulate requisite for the pseudo-spin/ $SU(2) \times U(1)$  model of emergent bilayered structures in honeycomb layered oxides.<sup>3,6,7</sup>

Fig. 2 shows the high-resolution optimum bright-field (OBF) STEM imaging of honeycomb layered  $\text{Na}_2\text{Zn}_2\text{TeO}_6$  successfully taken along the [100] and [110] zone axes. OBF-STEM images obtained along the [100] zone axis (Fig. 2a, b and e) shows an array of dull blue spots (Na atoms) sandwiched between slab planes of Te (larger bright yellow spots) and Ni (smaller yellow spots) atoms planes (light spots). The –Ni–Ni–Te–Ni–Ni– sequential arrangement of the Ni atoms and Te atoms, typical for honeycomb layered oxides,<sup>4,5,14</sup> is clearly visualised. In ordered honeycomb layered tellurates,<sup>2,5</sup> the Te atoms

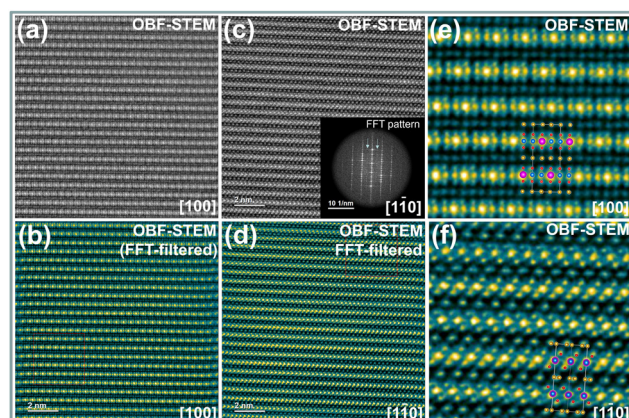
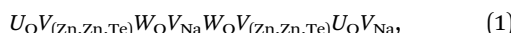


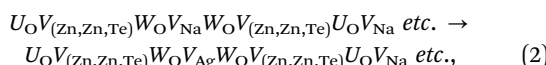
**Fig. 2** High-resolution optimum bright-field (OBF) STEM imaging of honeycomb layered  $\text{Na}_2\text{Zn}_2\text{TeO}_6$  along multiple zone axes. (a) OBF-STEM image of  $\text{Na}_2\text{Zn}_2\text{TeO}_6$  taken along [100] zone axis and (b) Corresponding fast Fourier-transform (FFT) filtered image. (c) OBF-STEM image of  $\text{Na}_2\text{Zn}_2\text{TeO}_6$  taken along [110] zone axis and (d) Corresponding fast Fourier-transform filtered image. Inset shows FFT image. (e) and (f) Atomic-resolution OBF-STEM images taken along the [100] and [110] zone axes. Atomistic structural models of  $\text{Na}_2\text{Zn}_2\text{TeO}_6$  acquired based on STEM analyses along the [100] and [110] zone axes have been embedded on the STEM images. Na atoms are shown in brown whilst Zn and Te atoms are shown in blue and pink, respectively. Oxygen atoms are shown in red.

(larger golden spots) are typically positioned directly below or above the adjacent slabs in idyllic vertical arrays. However, the enlarged OBF-STEM images taken along the [100] zone axis (Fig. 2e) reveal the slabs to deviate laterally from the ‘optimal’ arrays (as highlighted by the green and pink lines) in an alternating fashion across the slabs.

Moreover, OBF-STEM images obtained along the [110] zone axis (Fig. 2c, d and f) show the slab ordering in  $\text{Na}_2\text{Zn}_2\text{TeO}_6$ , wherein the oxygen atoms are arranged diagonally in a zig-zag orientation across the Zn and Te slabs. The slab stacking sequence can thus be represented in the FCC/HCP notation<sup>3</sup> as:



with  $W_\text{O}V_\text{Na}W_\text{O}$  representing prismatic coordination of Na atoms with oxygen atoms and  $V_{(\text{Zn},\text{Zn},\text{Te})}$  indicating that the Zn atoms are arranged in a two-dimensional (2D) honeycomb lattice with the sites at the centers of the honeycomb pattern occupied by Te atoms. Further, as per the FCC/HCP notation, Te and Zn atoms are octahedrally coordinated to oxygen atoms whereas Na atoms are prismatically coordinated. Reaction of  $\text{Na}_2\text{Zn}_2\text{TeO}_6$  with  $\text{AgNO}_3$  to yield  $\text{Ag}_2\text{Zn}_2\text{TeO}_6$  involves a topochemical transformation, wherein Na atoms (in prismatic coordination with oxygen) are replaced with Ag atoms (in prismatic coordination with oxygen) with the honeycomb arrangement of Zn atoms around Te maintained. In FCC/HCP notation, the topochemical transformation can be expressed as:



both with Na and Ag coordinated in a prismatic manner to O atoms. Generally, Ag-based honeycomb layered oxides (such as  $\text{Ag}_3\text{Ni}_2\text{SbO}_6$ ,<sup>15</sup>  $\text{Ag}_3\text{Zn}_2\text{SbO}_6$ ,<sup>15</sup> etc.) display linear/dumbbell coordination of Ag atoms with oxygen atoms.<sup>2</sup> However,  $\text{Ag}_2\text{Zn}_2\text{TeO}_6$  displays a prismatic coordination of Ag with O atoms (Fig. 1e and f), affirming the variegated coordination chemistry of monolayered Ag lattices as predicted by standard density functional theory (DFT) computations.<sup>16</sup>

Enlarged OBF-STEM images taken in both the [100] and [110] zone axes (Fig. 2e and f), reveal the Na-atom layers interposed between the Te and Zn slabs. Na atoms in the precursor material,  $\text{Na}_2\text{Zn}_2\text{TeO}_6$  (*i.e.*, prior to the topochemical reaction with molten  $\text{AgNO}_3$ ) are arranged in both honeycomb and hexagonal lattices, as seen in the magnified OBF-STEM images taken along the [110] zone axis (Fig. 3a). Honeycomb lattice arrangement of Na atoms,



manifests as double Na contrast spots arranged along the 2D slab, whereas hexagonal lattice arrangement of Na atoms ( $\text{U}_\text{O}V_{(\text{Zn},\text{Zn},\text{Te})}W_\text{O}V_\text{Na}W_\text{O}V_{(\text{Zn},\text{Zn},\text{Te})}U_\text{O}V_\text{Na}$ : see, eqn (1)) manifests as single Na contrast spots along the 2D slab.

It is worth noting that the varying intensity of the Na atom layers (particularly for hexagonal lattices) as seen in the magnified OBF-STEM images taken along the [110] zone axis (Fig. 3a), evince the occupation of Na atoms in distinct crystallographic sites with varying occupancies; typical for this class of

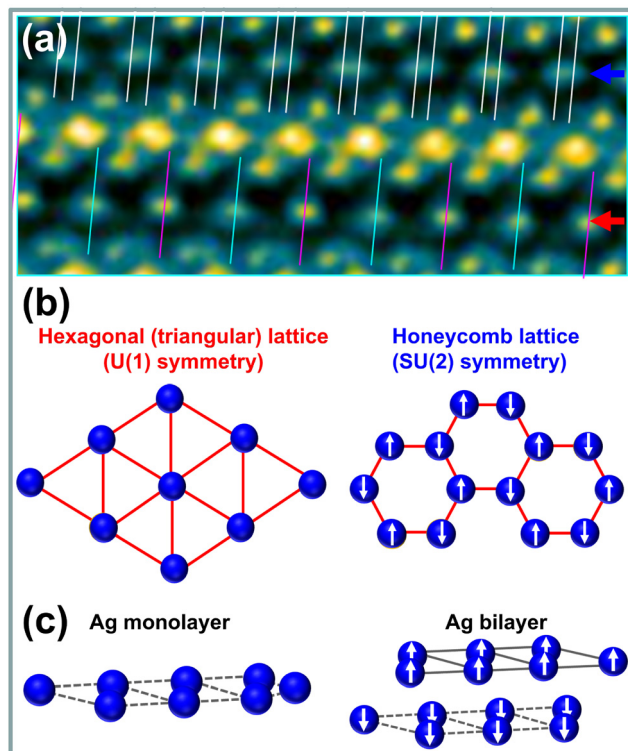


Fig. 3 Perceived monolayer–bilayer transition upon topotactic  $\text{Ag}^+$  reaction of honeycomb layered  $\text{Na}_2\text{Zn}_2\text{TeO}_6$  using molten  $\text{AgNO}_3$ . (a) Atomic resolution OBF-STEM image of  $\text{Na}_2\text{Zn}_2\text{TeO}_6$  taken along [1-10] zone axis showing honeycomb and hexagonal lattice arrangement of Na atoms. (b) Schematic of expected Ag atom arrangements upon topotactic  $\text{Ag}^+$  reaction of honeycomb layered  $\text{Na}_2\text{Zn}_2\text{TeO}_6$  using molten  $\text{AgNO}_3$  to form  $\text{Ag}_2\text{Zn}_2\text{TeO}_6$ . (c) Schematic of perceived monolayer–bilayer transition in  $\text{Ag}_2\text{Zn}_2\text{TeO}_6$  upon topotactic  $\text{Ag}^+$  reaction of honeycomb layered  $\text{Na}_2\text{Zn}_2\text{TeO}_6$  using molten  $\text{AgNO}_3$ .

tellurates.<sup>10,17–21</sup> In addition, there are different contrasts at Na hexagonal sites that should be crystallographically equivalent (shown in blue and pink slash lines in Fig. 3a), indicating a modulation in the occupancies (as can be affirmed from the fast Fourier-transform (FFT) image (Fig. 2c inset)).

Na atoms arranged in both hexagonal and honeycomb lattices in  $\text{Na}_2\text{Zn}_2\text{TeO}_6$  presents the material as a model for studying phenomena related to the pseudo-spin/ $SU(2) \times U(1)$  model,<sup>3,6,7</sup> particularly when the Na atoms in either lattice (hexagonal or honeycomb, albeit both monolayered) are replaced with Ag atoms, as is the case when  $\text{Na}_2\text{Zn}_2\text{TeO}_6$  undergoes the topochemical reaction with molten  $\text{AgNO}_3$ . For domains with monolayered hexagonal lattices (pre-topotactic ion exchange), Ag atoms are expected by the model<sup>3,6,7</sup> to align to form monolayers (post-topotactic ion exchange), consistent with the results displayed in Fig. 2 and 3(a) (pre-topotactic) and Fig. 1(a) (post-topotactic).

However, in the case of monolayered honeycomb lattices of Na, the topochemical reaction with Ag atoms re-align the monolayered honeycomb lattice to form Ag bilayers (as already observed in a previous publication<sup>6</sup> and illustrated in Fig. 3b and c). This re-alignment, attributed to the bifurcation of the honeycomb lattice is perceived (understood) as a

monolayer-to-bilayer transition, facilitated by *sd*-hybridisation.<sup>3,6,7</sup> Thus, the predominantly monolayered structure observed in the herein reported Ag-based honeycomb materials suggest the lack of *sd*-hybridisation of the Ag orbitals on the hexagonal lattice, contrary to the case on the honeycomb lattice. Finally, the minimal bilayered regions observed and reported in Fig. 1(a) can be attributed to the presence of minimal honeycomb lattice domains in the precursor  $\text{Na}_2\text{Zn}_2\text{TeO}_6$ , expected to favour *sd*-hybridisation restricted to these domains.

In summary, optimum bright-field scanning transmission electron microscopy (OBF-STEM) has been successfully utilised in this work to interrogate the local atomic structural information of the beam-sensitive honeycomb layered material,  $\text{Na}_2\text{Zn}_2\text{TeO}_6$ , thus attaining sub-angstrom spatial resolution. OBF-STEM reveals a commixture of hexagonal and honeycomb lattice arrangement of Na atoms in the precursor  $\text{Na}_2\text{Zn}_2\text{TeO}_6$ , accounting for the observation of mixed monolayer and bilayer arrangement of Ag atoms in  $\text{Ag}_2\text{Zn}_2\text{TeO}_6$  (prepared *via* topochemical ion-exchange of Na in  $\text{Na}_2\text{Zn}_2\text{TeO}_6$  with Ag atoms). These OBF-STEM results lend credence to the existence of exotic spin models/non-commutative gauge field theories on the honeycomb lattice (potentially absent on hexagonal and other non-honeycomb lattices) expected to greatly invigorate the experimental, theoretical and computational studies of monolayer-bilayer honeycomb layered oxides. Altogether, the success of OBF-STEM imaging of otherwise challenging honeycomb layered materials is envisaged to further advance the study of their structure–property relationships.

This work was supported by the AIST Edge Runners Funding and Japan Society for the Promotion of Science (JSPS KAKENHI Grant Numbers 24KF0275 and 23K04922).

## Conflicts of interest

There are no conflicts to declare.

## Data availability

The data supporting this article have been included as part of the ESI.†

## References

- G. M. Kanyolo, T. Masese, N. Matsubara, C.-Y. Chen, J. Rizell, Z.-D. Huang, Y. Sassa, M. Måansson, H. Senoh and H. Matsumoto, *Chem. Soc. Rev.*, 2021, **50**, 3990–4030.
- G. M. Kanyolo, T. Masese, A. Alshehabi and Z.-D. Huang, *Mater. Today Chem.*, 2023, **33**, 101657.
- G. M. Kanyolo, T. Masese, Y. Miyazaki, S. Tachibana, C. Zhong, Y. Oriksa and T. Saito, *Prog. Mater. Sci.*, 2024, **141**, 101205.
- T. Masese, Y. Miyazaki, J. Rizell, G. M. Kanyolo, T. Takahashi, M. Ito, H. Senoh and T. Saito, *Materialia*, 2021, **15**, 101003.
- T. Masese, Y. Miyazaki, G. Mbiti Kanyolo, T. Takahashi, M. Ito, H. Senoh and T. Saito, *ACS Appl. Nano Mater.*, 2021, **4**, 279–287.
- T. Masese, G. M. Kanyolo, Y. Miyazaki, M. Ito, N. Taguchi, J. Rizell, S. Tachibana, K. Tada, Z.-D. Huang and A. Alshehabi, *et al.*, *Adv. Sci.*, 2023, **10**, 2204672.
- G. M. Kanyolo and T. Masese, *Mater. Today Phys.*, 2023, **39**, 101271.
- S. Komori, K. Tada, N. Taguchi, T. Taniyama and T. Masese, *J. Mater. Chem. C*, 2023, **11**, 11213–11217.
- J.-F. Wu, Q. Wang and X. Guo, *J. Power Sources*, 2018, **402**, 513–518.
- Y. Li, Z. Deng, J. Peng, E. Chen, Y. Yu, X. Li, J. Luo, Y. Huang, J. Zhu and C. Fang, *et al.*, *Chem. – Eur. J.*, 2018, **24**, 1057–1061.
- K. Ooe, T. Seki, K. Yoshida, Y. Kohno, Y. Ikuhara and N. Shibata, *Sci. Adv.*, 2023, **9**, eadf6865.
- K. Ooe, T. Seki, M. Nogami, Y. Ikuhara and N. Shibata, *Microscopy*, 2024, dfae051.
- Z. Wang, *J. Phys. Chem. B*, 2000, **104**(6), 1153–1175.
- T. Masese, Y. Miyazaki, J. Rizell, G. M. Kanyolo, C.-Y. Chen, H. Ubukata, K. Kubota, K. Sau, T. Ikeshoji and Z.-D. Huang, *et al.*, *Nat. Commun.*, 2021, **12**, 4660.
- R. Nagarajan, S. Uma, M. Jayaraj, J. Tate and A. Sleight, *Solid State Sci.*, 2002, **4**, 787–792.
- K. Tada, T. Masese and G. M. Kanyolo, *Comput. Mater. Sci.*, 2022, **207**, 111322.
- M. A. Evstigneeva, V. B. Nalbandyan, A. A. Petrenko, B. S. Medvedev and A. A. Kataev, *Chem. Mater.*, 2011, **23**, 1174–1181.
- R. Salgado, S. Terny and M. A. Frechero, *Mater. Sci. Eng. B*, 2025, **312**, 117865.
- K. Yamamoto, Y. Ono and R. Inada, *Heliyon*, 2024, **10**, e30691.
- H. Huang, Y. Yang, C. Chi, H.-H. Wu and B. Huang, *J. Mater. Chem. A*, 2020, **8**, 22816–22827.
- J.-F. Wu, Z.-Y. Yu, Q. Wang and X. Guo, *Energy Storage Mater.*, 2020, **24**, 467–471.